Electronic Supplementary Information

Alternating current properties of bulk- and nanosheet-graphitic carbon nitride compacts at elevated temperatures

Tosapol Maluangnont,[a]* Phieraya Pulphol,[b] Kanokwan Chaithaweep,[c]

Klichchupong Dabsamut,[d] Thawanrat Kobkeatthawin,[e] Siwaporn Meejoo Smith,[e]

Adisak Boonchun,[d] and Naratip Vittayakorn[c]

[a] Electroceramics Research Laboratory, College of Materials Innovation and Technology, King Mongkut's Institute of Technology Ladkrabang, Bangkok 10520, Thailand

[b] Department of Materials Science, Faculty of Science, Srinakharinwirot University, Bangkok 10110, Thailand

[c] Advanced Materials Research Unit and Department of Chemistry, School of Science, King Mongkut's Institute of Technology Ladkrabang, Bangkok 10520, Thailand

[d] Department of Physics, Faculty of Science, Kasetsart University, Bangkok 10900, Thailand

[e] Center of Sustainable Energy and Green Materials and Department of Chemistry, Faculty of Science, Mahidol University, Nakhon Pathom 73170, Thailand
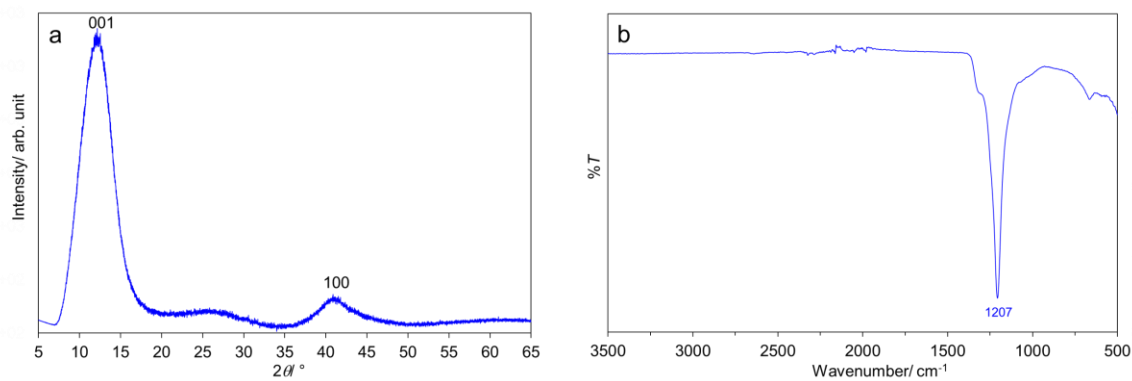
*corresponding author email: tosapol.ma@kmitl.ac.th

Figure S1   (a) XRD pattern, and (b) FTIR spectrum of graphite fluoride.

The XRD pattern in Figure S1a shows two board peaks at $2\theta = 12.3°$ ($d = 7.2$ Å, *i.e.,* the interlayer distance), and $2\theta = 40.7°$ ($d = 2.2$ Å). These peaks are assigned as the 001 and 100 reflections, respectively, typical for graphite fluoride which has a turbostatic structure.[1] Figure S1b is the IR spectrum, showing strong peak at 1207 cm^{-1} typical of the C-F stretching.[2]
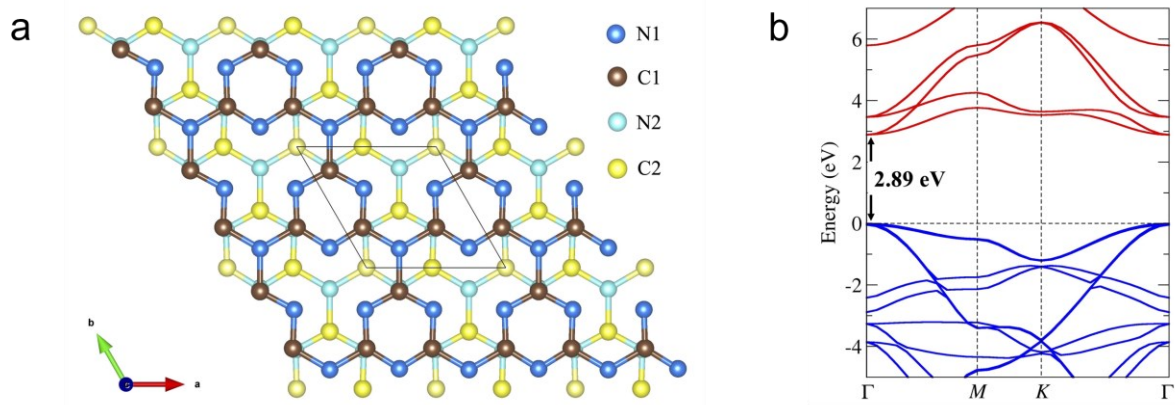
Figure S2   (a) Crystal structure on the *ab* plane, and (b) electronic band structure of bulk-g–C_3N_4. Blue and brown balls are nitrogen (N1) and carbon (C1) at the top layer, while light blue and yellow balls represent nitrogen (N2) and carbon (C2) at the bottom layer.

We employed the *s*-triazine-based unit as the structure of bulk-g–C_3N_4 as shown in Figure S2a, with the layers stacked in the A-B fashion.[3] The calculated lattice constants of bulk-g–C_3N_4 are $a = b = 4.741$Å, $c = 6.626$ Å consistent with the reported values.[3] Figure S2b presents the electronic band structure of bulk-g–C_3N_4 obtained using the HSE06 functional. It is found that bulk-g–C_3N_4 exhibited a direct bandgap semiconductor behavior, with an energy gap of 2.89 eV. This is close to the reported values of 2.73 and 2.88 eV calculated by the same functional.[3]

Table S1   Comparison of CTE obtained in this work vs those of related materials reported in the literature.[a]

Sample	α/ K^{-1}	Method[b]	T range/°C	Ref.
Bulk-g–C_3N_4	$3.1\times10^{-5}/2.5\times10^{-5}$	vT-XRD	25-350	This work
Nanosheet-g–C_3N_4	$2.2\times10^{-5}/2.4\times10^{-5}$	vT-XRD	25-350	This work
Bulk-g–C_3N_4	1×10^{-5}-2.5×10^{-5}	DFT calculation	25-400	Sun et al[4]
Amorphous carbon nitride	2×10^{-6}-9×10^{-6}	TIB	NA	Champi et al[5]
Natural graphite sheet	3.3×10^{-5}	TMA	30-100	Cermak et al[6]
hBN	3.77×10^{-5}	vT-XRD	24.5	Paszkowicz et al[7]

[a]values in this work listed as heating/cooling

[b]vt-XRD: variable-temperature XRD

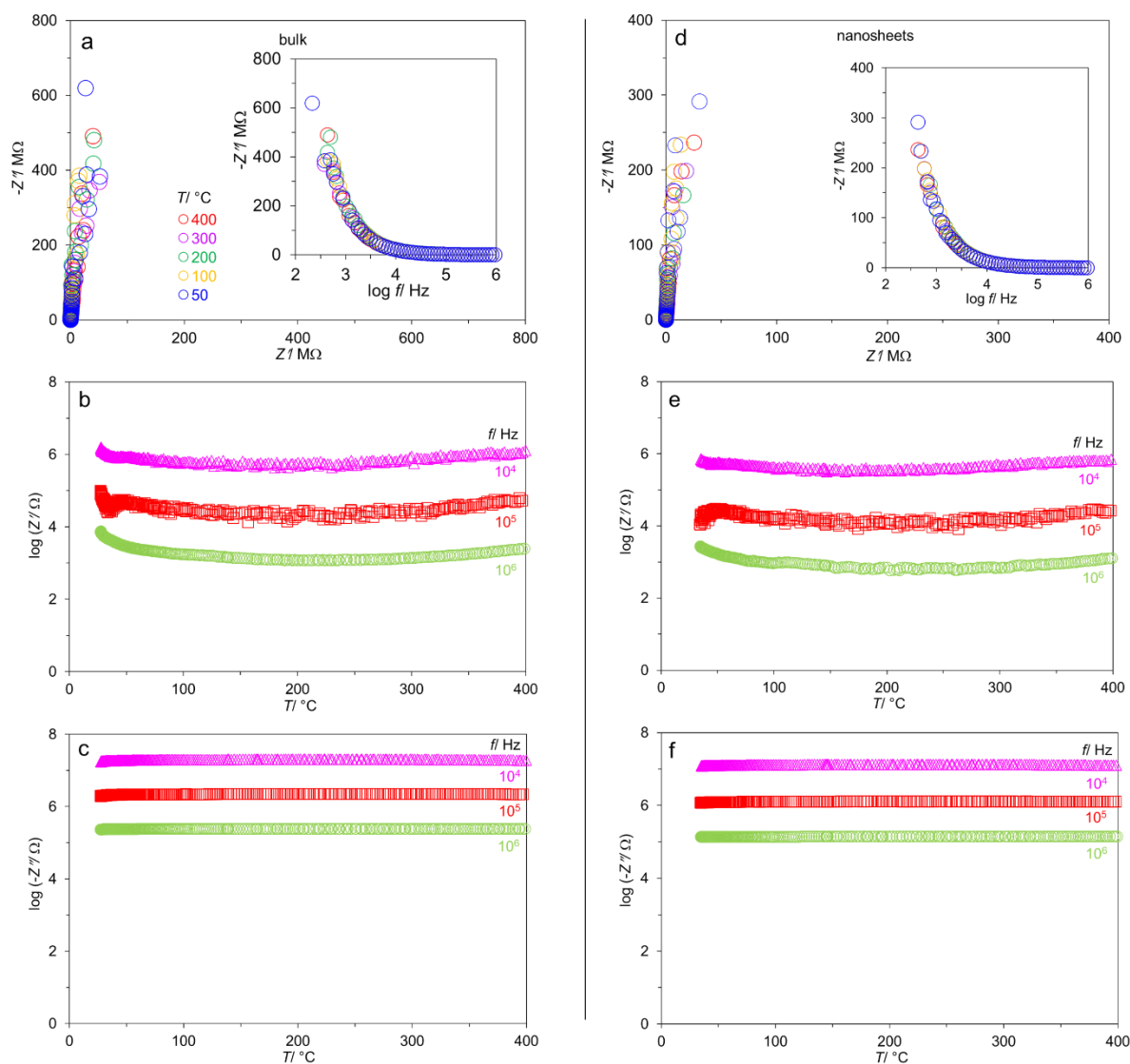TMA: thermomechanical analysis

TIB: thermally induced bending

Figure S3   (a,d) Nyquist plots measured at different temperatures; and the temperature dependence of (b,e) log Z', and (c,f) log $-Z''$ at selected frequencies. Panel (a-c) for bulk-g–C_3N_4, while panel (d-f) for nanosheet-g–C_3N_4. Data were obtained in the cooling process.

The Nyquist plots of both samples appeared almost as the straight lines from 400→50 °C, indicating their highly insulating nature consistent with the literature.[8] This is also evident from the flat T-dependence of log Z and log $-Z''$ in Figure S1b,c,e, and f. The spectroscopic plots in the inset (i.e., $-Z''$ vs log f) are also featureless. Apparently, it is not possible to extract more information from the f-scanning results.
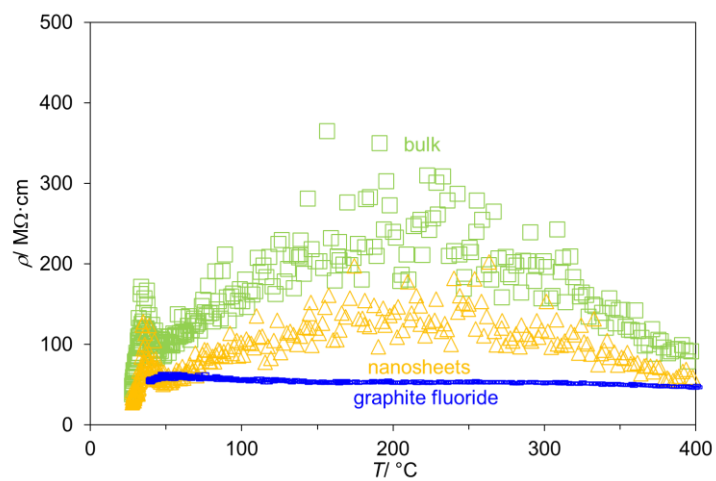
Figure S4   Variation of resistivity ρ (in MΩ·cm) of the bulk- and nanosheet-g–C_3N_4 in comparison to graphite fluoride. Data shown here were at 10^5 Hz and were obtained in the cooling process.
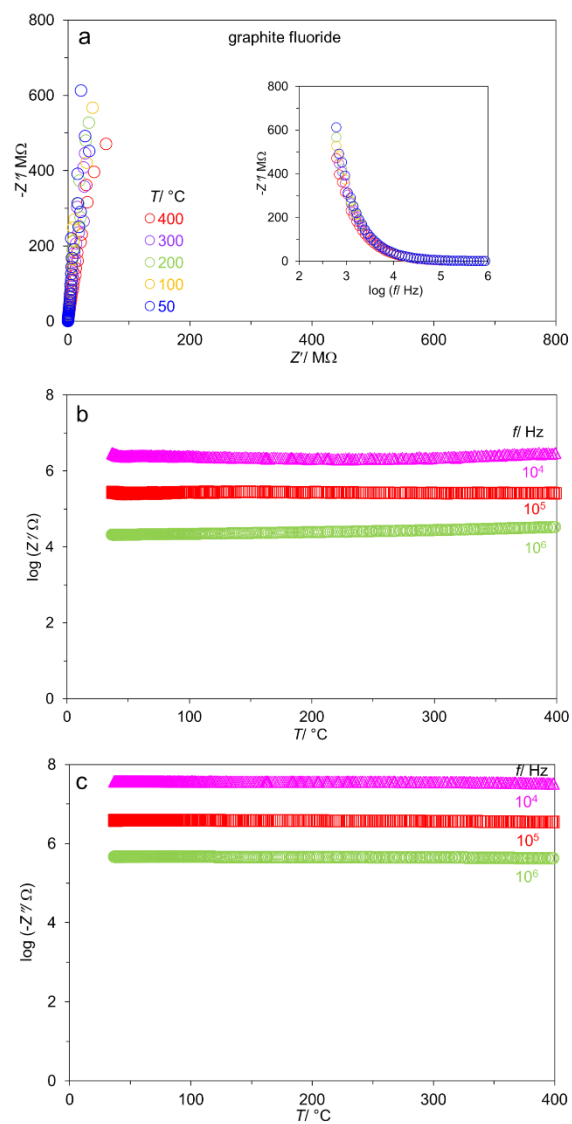
Figure S5   (a) Nyquist plots of graphite fluoride measured at different temperatures; and the temperature dependence of (b) log Z', and (c) log $-Z''$ at selected frequencies. Data were obtained in the cooling process.

Calculation of AC properties

The complex impedance Z^* is described by:

$$Z^* = Z' + iZ'' \tag{S1}$$

with Z' and Z'' as the real and imaginary part of the function, respectively. The resistivity ρ ($\Omega \cdot$cm) can be calculated from Z^*:

$$\rho = 1/\sigma \tag{S2}$$

$$\sigma = (t/A) \cdot [Z'/(Z'^2 + Z''^2)] \tag{S3}$$

where σ is the conductivity (S$\cdot$cm^{-1}), t is the thickness of the pellet in cm (i.e., the distance between electrodes in cm), and A is the area of the pellet in cm^2.

The complex dielectric permittivity ε^* [eq(S4)] was calculated using eqs (S5-S7):

$$\varepsilon^* = \varepsilon' + i\varepsilon'' \tag{S4}$$

$$\varepsilon' = (t/\omega A \varepsilon_0) \cdot [Z''/(Z'^2 + Z''^2)] \tag{S5}$$

$$\varepsilon'' = (t/\omega A \varepsilon_0) \cdot [Z'/(Z'^2 + Z''^2)] \tag{S6}$$

$$\tan \delta = \varepsilon''/\varepsilon' \tag{S7}$$

with ε' and ε'' as the real- and imaginary part of the complex dielectric function; $\omega = 2\pi f$; ε_0 is the vacuum permittivity (8.854×10^{-12} F$\cdot$m^{-1}); and $\tan \delta$ is the loss tangent.

The refractive index[9, 10] n, dielectric heating coefficient[9, 11] J, and attenuation coefficient[12-14] α were calculated using eq(S8), (S9), and (S10), respectively (where c is the speed of light):

$$n^2 = [(\varepsilon'^2 + \varepsilon''^2)^{1/2} + \varepsilon']/2 \tag{S8}$$

$$J = 1/(\varepsilon' \cdot \tan \delta) \tag{S9}$$

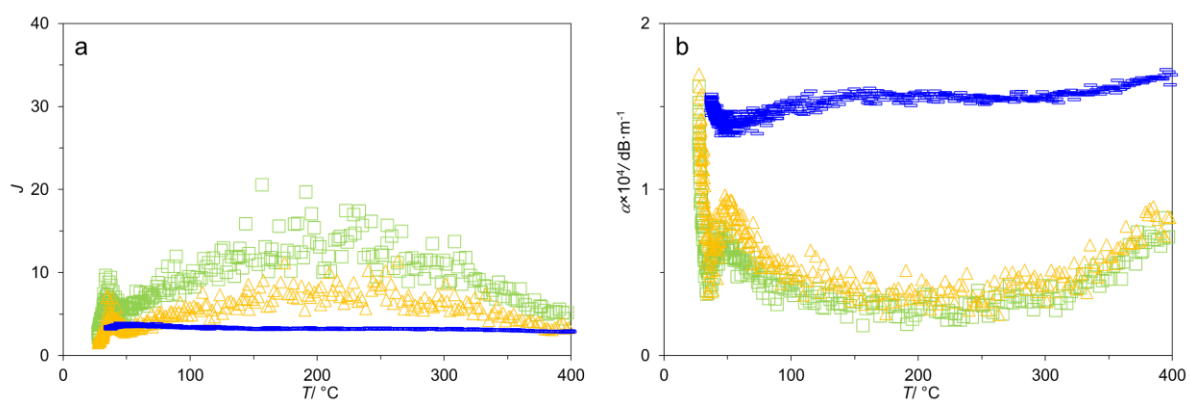$$\alpha = \frac{2\pi f}{\sqrt{2}c} \sqrt{-\varepsilon' + \sqrt{(\varepsilon'^2 + \varepsilon''^2)}} \tag{S10}$$

Figure S6   Temperature dependence of (a) dielectric heating coefficient J, and (b) attenuation coefficient $\alpha \times 10^4$, for bulk and nanosheets samples of g–C$_3$N$_4$, in comparison to graphite fluoride. Data shown here were at 10^5 Hz and were obtained in the cooling process.

To provide more examples on the T-dependence of electrical properties in g–C$_3$N$_4$, we calculated the dielectric heating coefficient J [eq(S9)] and the attenuation coefficient α [eq(S10)]. As shown in Figure S6a at $f = 10^5$ Hz, J of graphite fluoride is low (3.2) and relatively constant from 400 to 50 °C. On the other hand, the J values of g–C$_3$N$_4$ samples are larger (averaged 7.7-13.1) and more scatter with T. For comparison, at 10^5 Hz and RT, J of the cellulose film[9] is ~30.

Figure S6b shows the T-dependence of α at 10^5 Hz (α is the ability of a material to suppress electromagnetic waves). The α values are relatively constant for graphite fluoride (1.5×10^{-4}) compared to those with larger T-variations for g–C$_3$N$_4$ samples (2.8×10^{-5}). For comparison, α of ceramics such as layered titanate is on the order of 10^{-3}.[12]

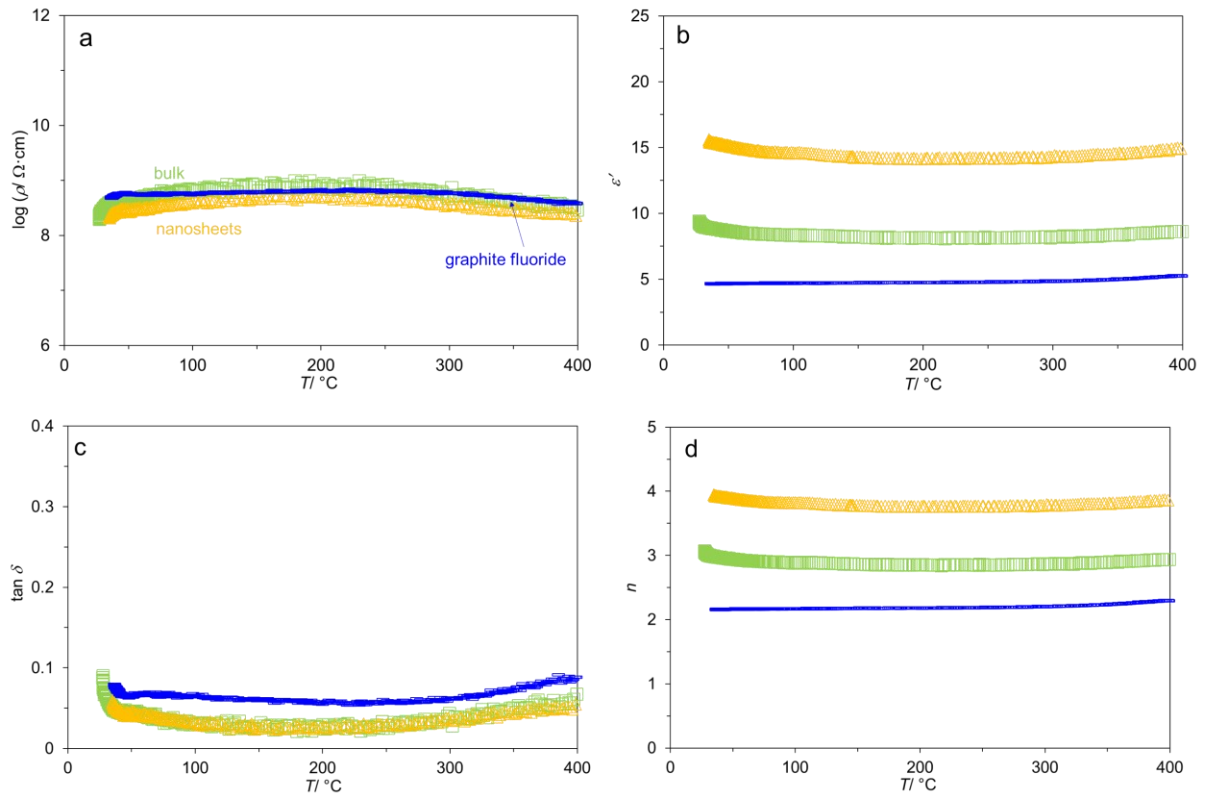Figure S7   Temperature dependence of (a) log ρ, (b) ε', (c) tan δ, and (d) n for bulk and nanosheets samples of g–C$_3$N$_4$, in comparison to graphite fluoride. Data shown here were at 10^4 Hz and were obtained in the cooling process.

Figure S8　　　Temperature dependence of (a) log ρ, (b) ε', (c) tan δ, and (d) n for bulk and nanosheets samples of g–C_3N_4, in comparison to graphite fluoride. Data shown here were at 10^3 Hz and were obtained in the cooling process.
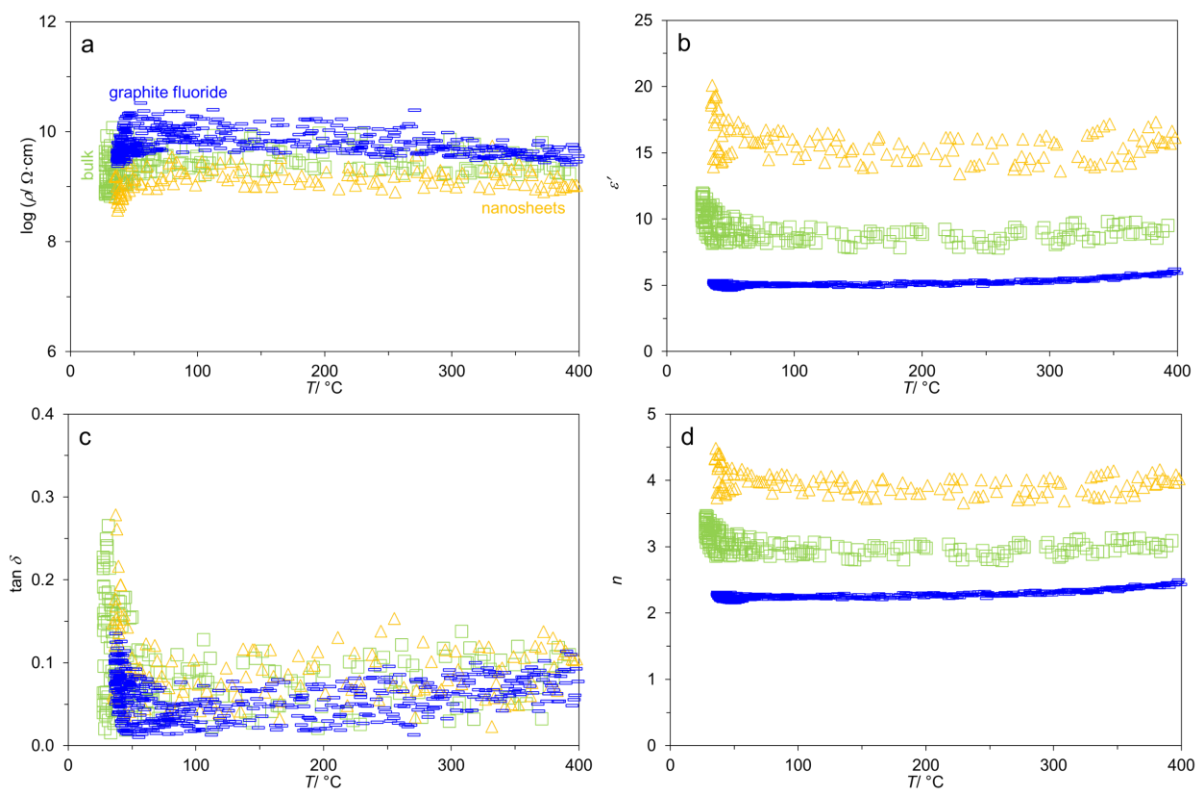
The data at 10^3 Hz are noisy compared to those at 10^4 and 10^5 Hz. Presumably, at low frequency the charge conduction is so small and almost reach the instrument limit. (Yet, it is apparent that the average values are consistent with those reported in Table 2 in the manuscript.) The data at 10^2 Hz were also collected, scattering heavily, presumably due to the contribution from electrode polarization typically observed at low-frequency. These are not reported here.

Supplementary references

(1) Kita, Y.; Watanabe, N.; Fujii, Y. Chemical composition and crystal structure of graphite fluoride. *J. Am. Chem. Soc.* **1979**, *101*, 3832-3841.
(2) Kang, W.; Li, S. Preparation of fluorinated graphene to study its gas sensitivity. *RSC Adv.* **2018**, *8*, 23459-23467.
(3) Zhu, B.; Cheng, B.; Zhang, L.; Yu, J. Review on DFT calculation of s-triazine-based carbon nitride. *Carbon Energy* **2019**, *1*, 32-56.
(4) Sun, S. P.; Gu, S.; Sun, J. H.; Xia, F. F.; Chen, G. H. First principles investigation of the electronic properties of graphitic carbon nitride with different building block and sheet staggered arrangement. *J. Alloys Compd.* **2018**, *735*, 131-139.
(5) Champi, A.; Lacerda, R. G.; Marques, F. C. Thermal expansion coefficient of amorphous carbon nitride thin films deposited by glow discharge. *Thin Solid Films* **2002**, *420-421*, 200-204.
(6) Cermak, M.; Perez, N.; Collins, M.; Bahrami, M. Material properties and structure of natural graphite sheet. *Sci. Rep.* **2020**, *10*, 18672.
(7) Paszkowicz, W.; Pelka, J. B.; Knapp, M.; Szyszko, T.; Podsiadlo, S. Lattice parameters and anisotropic thermal expansion of hexagonal boron nitride in the 10–297.5 K temperature range. *Appl. Phys. A* **2002**, *75*, 431-435.
(8) Maluangnont, T.; Pulphol, P.; Pongampai, S.; Kobkeatthawin, T.; Smith, S. M.; Vittayakorn, N. TiO_2/graphitic carbon nitride nanosheet composite with enhanced sensitivity to atmospheric water. *RSC Adv.* **2023**, *13*, 6143-6152.
(9) Maluangnont, T.; Sriphan, S.; Charoonsuk, T.; Vittayakorn, N. Dielectric spectroscopy and electric modulus analyses of $Ti_{0.8}O_2$ nanosheets–Ag nanoparticles–cellulose filter paper composites. *Integr. Ferroelectr.* **2022**, *224*, 214-224.
(10) Andoulsi-Fezei, R.; Sdiri, N.; Horchani-Naifer, K.; Férid, M. Effect of temperature on the electrical properties of lanthanum ferrite. *Spectrochim. Acta A* **2018**, *205*, 214-220.
(11) Anju, V. P.; Manoj, M.; Mohanan, P.; Narayanankutty, S. K. A comparative study on electromagnetic interference shielding effectiveness of carbon nanofiber and nanofibrillated cellulose composites *Syn. Met.* **2019**, *247*, 285-297.
(12) Sriphan, S.; Pulphol, P.; Charoonsuk, T.; Maluangnont, T.; Vittayakorn, N. Effect of adsorbed water and temperature on the universal power law behavior of lepidocrocite-type alkali titanate ceramics. *J. Phys. Chem. C* **2021**, *125*, 12910–12920.
(13) Kułacz, K.; Orzechowski, K. Nontronite and intercalated nontronite as effective and cheap absorbers of electromagnetic radiation. *Dalton Trans.* **2019**, *48*, 3874-3882.
(14) Chung, D. D. L. Materials for electromagnetic interference shielding. *J. Mater. Eng. Perform.* **2000**, *9*, 350-354.